**OPEN**

Correspondence and
requests for materials
should be addressed to
K.T. (terao@eng.
kagawa-u.ac.jp)

# Subcellular glucose exposure biases the spatial distribution of insulin granules in single pancreatic beta cells

Kyohei Terao[1], Murat Gel[2], Atsuhito Okonogi[3], Ariko Fuke[3], Teru Okitsu[4], Takashi Tada[5], Takaaki Suzuki[1], Shinya Nagamatsu[6], Masao Washizu[7] & Hidetoshi Kotera[3]

[1]Department of Intelligent Mechanical Systems Engineering, Kagawa University, Takamatsu 761-0396, Japan, [2]CSIRO, Material Science and Engineering, Clayton, VIC 3030, Australia, [3]Department of Microengineering, Kyoto University, Kyoto 606-8501, Japan, [4]Institute of Industrial Science, The University of Tokyo, Tokyo 153-8904, Japan, [5]Institute for Frontier Medical Sciences, Kyoto University, Kyoto 606-8507, Japan, [6]Department of Biochemistry, Kyorin University School of Medicine, Tokyo 181-8611, Japan, [7]Department of Mechanical Engineering, The University of Tokyo, Tokyo 113-8656, Japan.

In living tissues, a cell is exposed to chemical substances delivered partially to its surface. Such a heterogeneous chemical environment potentially induces cell polarity. To evaluate this effect, we developed a microfluidic device that realizes spatially confined delivery of chemical substances at subcellular resolution. Our microfluidic device allows simple setup and stable operation for over 4 h to deliver chemicals partially to a single cell. Using the device, we showed that subcellular glucose exposure triggers an intracellular [Ca²⁺] change in the β-cells. In addition, the imaging of a cell expressing GFP-tagged insulin showed that continuous subcellular exposure to glucose biased the spatial distribution of insulin granules toward the site where the glucose was delivered. Our approach illustrates an experimental technique that will be applicable to many biological experiments for imaging the response to subcellular chemical exposure and will also provide new insights about the development of polarity of β-cells.

C
ells in a living body assemble in three-dimensional tissue structures. Such an *in vivo* situation intrinsically limits the space for the diffusion of chemical substances. This causes partial exposure of the cell to chemicals (e.g., hormones, blood glucose, and drugs) at its surface. It is thought that a cell senses such nonuniform chemical concentration and forms a heterogeneous intracellular structure using the nonuniformity as an external cue[1,2]. This phenomenon is known as cell polarity and is essential for cells with respect to exhibiting and maintaining function in a living body, for processes such as hormone production, apoptosis, proliferation, and differentiation[3]. Nevertheless, little is known about the environment that induces the cell polarity and its mechanism because of the lack of technology for reproducing such a heterogeneous chemical environment surrounding single cells. The realization of such a situation *in vitro* requires the spatially confined delivery of chemicals to a limited area of single cell surface. We have referred to this hereafter as "subcellular chemical delivery."

Common biological experiments handle cells as a mass in a bulk solution. In this situation, the chemical substances inevitably diffuse in the solution to reach a uniform concentration. Several groups have developed microfluidic devices for the partial delivery of chemicals to cells, including microfluidic focusing channels[4–6], microfluidic probes[7,8], and nanopipettes[9,10]. However, these devices still have the drawback of diffusion because they produce a gentle concentration gradient over the cell surface and do not have subcellular and stable delivery. To overcome this drawback, we developed a novel microfluidic device that allows us to deliver chemicals to single cells and to observe their intracellular responses.

We targeted a pancreatic β-cell that plays an important role in the regulation of the blood glucose level in the living body. A β-cell secretes insulin in response to the rise of glucose concentration in the blood. The cells form a cytoarchitecture known as a pancreatic islet, where each cell faces both a venous and an arterial capillary. A β-cell is known to have cell polarity in a living islet: intracellular insulin granules are biased toward the side facing the venous capillary[11]. It has been over 20 years since the morphological evidence was first reported; nevertheless, there is little understanding of the factors that induce the biased granule distribution and of the mechanism and the significance in a living body[12].

To verify the effect of subcellular glucose exposure from the blood capillary, we reproduced the *in vivo* scenario using our microfluidic device, delivered glucose to a limited area of a single β-cell, and observed its insulin granules. First, we evaluated the flow in the microfluidic device; then, we checked how a β-cell responds to the subcellular glucose exposure by observing the intracellular $[Ca^{2+}]$ change; and finally, we visualized the shift in the distribution of insulin granules.

Subcellular chemical delivery is performed with two microchannels (Ch1 and Ch2) separated by a solid wall with a lateral micro-orifice smaller than a cell (Fig. 1). A cell in Ch2 is first trapped at the micro-orifice by the flow from Ch2 to Ch1, where the pressure in Ch2 is higher than that in Ch1. The trapped cell is allowed to adhere to the channel and to spread at the orifice and seal it. The chemical substances are introduced into Ch1 for partial delivery to the cell surface. The consequent responses are visualized by optical microscopy. This technique allows a subcellular chemical delivery with a constant concentration over time without diffusion of chemicals and disturbance of the boundary between the solution of Ch1 and Ch2, because the solid wall physically separates them.

## Results

**Microfluidic device.** The design of the device and the calculated pressure in it are shown in Fig. 2a. The microfluidic device has two inlets and one outlet, which are driven by a single pump for the cell trapping and the subcellular delivery. The suction from the outlet spontaneously generates a pressure difference between Ch1 and Ch2, which linearly increases in accordance with the flow rate ($Q$) at the outlet. The pressure in Ch1 is kept lower than that in Ch2 around the orifices, inducing the flow from Ch2 to Ch1 through the orifices. This flow brings the cells in Ch2 toward the orifices and its pressure traps them there. When the cells are trapped, the orifices are closed and the pressure $P_{cell}$ is applied to them, which is also linearly increased with $Q$ (Fig. 2b) and was estimated to be in the range of 0–20 Pa under our experimental conditions. The experimental result indicates that the flow through the orifices was spontaneously induced (Fig. 2c), showing a good agreement with the simulation result.

After cell trapping, we verified the stability of the flow by adding a fluorescent solution, calcein-AM red orange, into Ch1 (Fig. 2e and f). Once a calcein-AM molecule enters the cell, it converts to a membrane-impermeable form. Thus, a cell emits fluorescence gradually while accumulating the fluorescent molecules. This process was visualized in the microdevice as shown in Supplementary Movie 1. The fluorescence of the cell gradually increased, showing successful subcellular chemical delivery without leakage and backflow of the solution.

The stability of the flow was monitored for 4 h. Regions of interest (ROIs) were set in Ch1 and Ch2 around the orifice, except around the cells (Fig. 2e). If the flow (nonfluorescent solution) leaks to Ch1, the Ch2 fluorescence in the magenta solid circle will decrease. On the other hand, the backflow (flow from Ch1 to Ch2) causes the increase of fluorescence in Ch2 in the white dotted circle. The results show almost stable fluorescence intensities in both channels (Fig. 2f). Although we detected a small fluctuation, the concentration of the Ch1 area was still kept 40 times higher than that of the Ch2 for 4 h.

**$[Ca^{2+}]$ response.** We checked the response of a β-cell to partially-delivered glucose using our microfluidic device by observing the changes in the intracellular $[Ca^{2+}]$. The time course after the
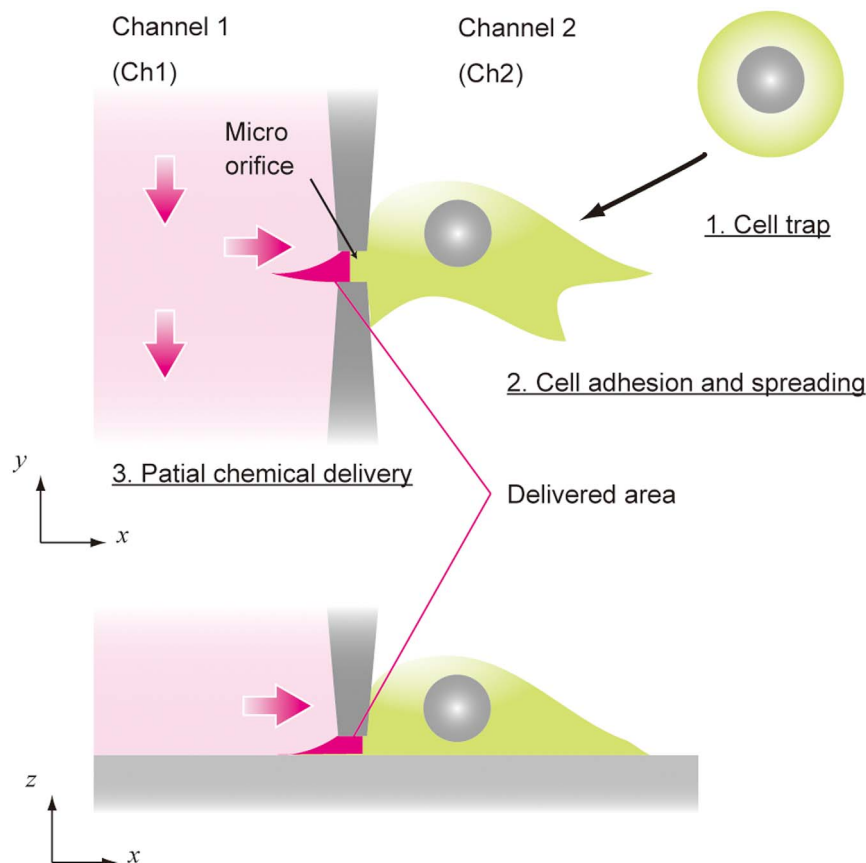


**Figure 1 | Concept of subcellular chemical delivery.** The two microchannels are separated by a thin vertical wall with a lateral micro-orifice smaller than the size of the target cell. The cells are applied to microchannel Ch2; one of them is trapped at the micro-orifice by the flow through it (1. cell trap) and is then allowed to spread on the substrate to seal the orifice (2. cell adhesion and spreading). The chemical substances are applied to the microchannel (Ch1) and delivered to a limited area of the cell surface (3. subcellular delivery). The cellular responses are observed by optical microscopy.
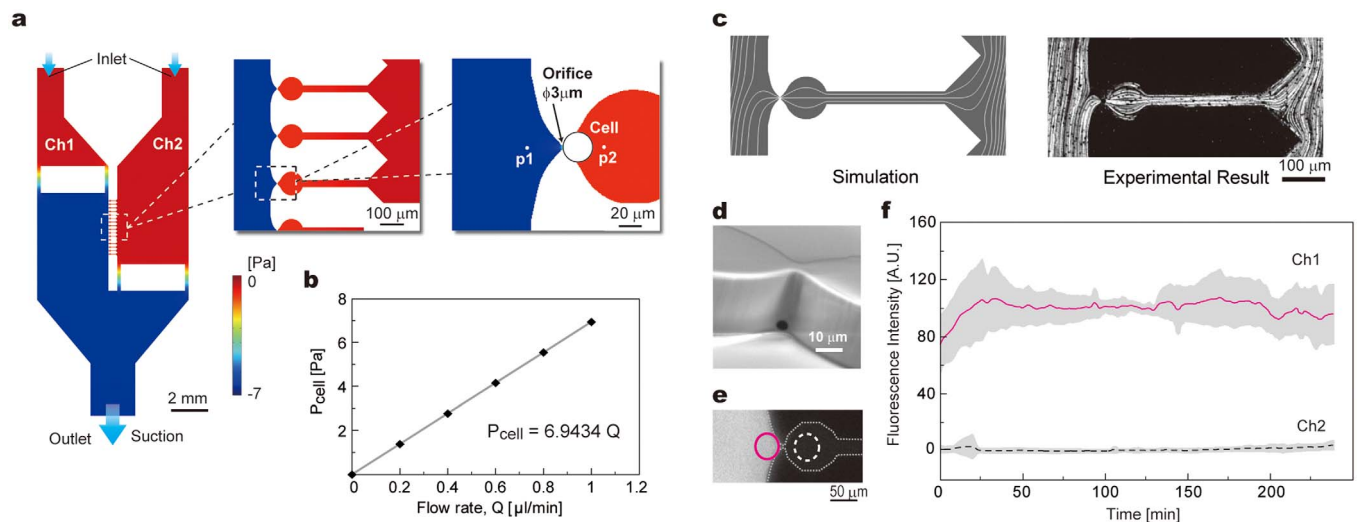
**Figure 2 | Microfluidic device for subcellular chemical delivery.** (a) Microfluidic channel design and the pressure map in the 2-μL/min suction from the outlet. (b) Linear increase of the pressure difference ($P_{cell} = p2 - p1$) applied to a trapped cell in accordance with the flow rate $Q$ at the outlet. (c) Streamlines in the device. Simulation and experimental results (the traces of the fluorescent particles were visualized). Scale bars: 100 μm. (d) The circular orifice in the vertical PDMS wall (SEM image). Scale bar: 10 μm. (e) Fluorescence image during the delivery of the calcein AM-red orange solution in Ch1. The magenta solid circle shows the area in Ch1 around the orifice. The white dotted circle shows the Ch2 area outside the trapped cell. Scale bar: 50 μm. (f) Time courses of the fluorescent intensity of Ch1 and Ch2 shown in the ROIs in e. Lines and gray areas show the plots of the mean values and the error bars (standard deviation, S.D.), respectively. The fluorescent solution was supplied to the reservoirs at $t \approx 130$ min. N = 13.

subcellular glucose delivery was visualized by a fluorescent [Ca²⁺] indicator, Fluo-8 (Fig. 3) by calculating the $F/F_0$ ratio. The lines and the gray areas in Fig. 3b show the mean values and the standard deviation (S.D.), respectively. After the cells were exposed to high glucose solution, their fluorescence intensities gradually increased 1.5 times higher than that at the initial state until $t = 200$ s and reached a plateau. In negative controls (0 mM glucose), the fluorescent intensity decreased slightly due to photo-bleaching.

**Spatial distribution of insulin granules.** The visualization of the insulin granules requires fluorescence labeling. Nagamatsu's group developed an insulin-GFP vector and reported the visualization of insulin granules and their secretion events[17–19]. However, it is a transient expression that has a relatively low yield of transfection

(e.g., ~10% by lipofection). Although it works in conventional bulk experiments where a large number of cells can be observed at once, the device proposed here gives a small number of trapped cells, requiring a high yield of transfection to realize a feasible experimental operation. This led us to establish a stable-expressing cell line (MIN6m9-C4, Supplementary Data 1).

Using insulin-GFP expressing cells, we observed the shifts of the spatial distribution of the insulin granules in response to the subcellular glucose exposure for 4 h (Fig. 4). The reason we selected the exposure time is that for 4 h, the cells are alive in the buffer solution and the flow is stable. The white area in Fig. 4 shows the fluorescence of insulin-GFP. As shown in the figure, the insulin granules were shifted towards the glucose exposure site. To estimate the distribution quantitatively, we set the $x$-$y$ coordinate as shown in the figure
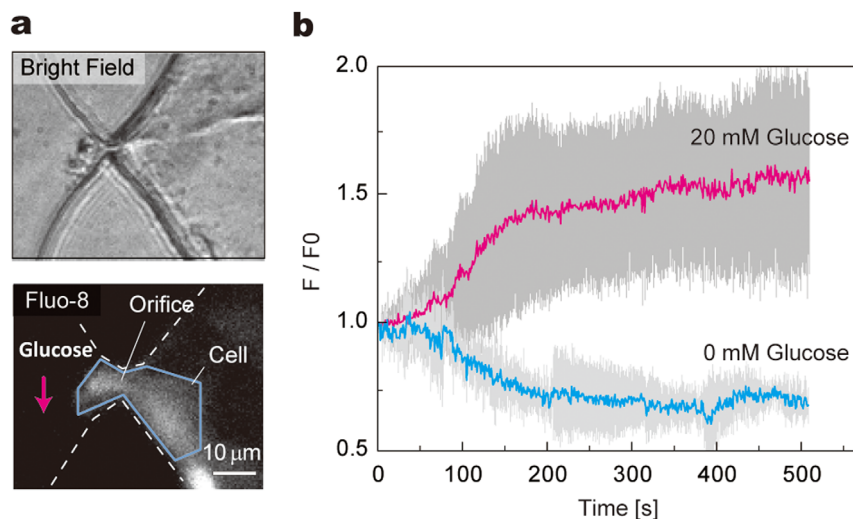


**Figure 3 | Intracellular [Ca²⁺] change after subcellular glucose delivery.** (a) Bright field and fluorescence images of the cell. Cells were stained by a calcium indicator, Fluo-8. Scale bars: 10 μm. (b) Time course of the fluorescent intensity ($F/F_0$) after glucose stimulation. The plots show the subcellular delivery of 20 mM glucose and no glucose delivery (0 mM glucose in the graph). The solid lines and gray areas show the plot of the mean values and the standard deviation (S.D.), respectively. N = 12.

**Figure 4 | Fluorescence images of intracellular insulin-GFP granules before (0 h) and after subcellular glucose exposure (4 h).** Six representative cells are shown. White areas refer to insulin-GFP fluorescence signal. The areas of the orifices are indicated by magenta squares. Scale bar: 20 μm.

and the center of the orifice as the origin. We traced the outlines of the glucose-delivered cells and calculated the $x$ positions of their centroids (center of the cell outline, $X_{cell}$). We also calculated the center of mass of an insulin granule image (center of the granule distribution, $X_{granule}$). To minimize the effect of cell deformation during the glucose exposure, the relative positions, $X'_{granule} = X_{granule} - X_{cell}$, were evaluated. We compared the $X'_{granule}$ 4 h after the partial glucose exposure with the initial state. The results are shown in Fig. 5 (25 mM/0 mM), in which they compared to those of the control experiments; both channels contained 25 mM glucose (25 mM/25 mM: whole cell stimulation) and no glucose (0 mM/ 0 mM: no stimulation). We performed these control experiments to evaluate the physical effect caused by the assymmetric microchannel structure because a trapped cell possibly senses such heterogeneous physical environment.

The $x$ shift of the distribution was $-4.78 \pm 4.20$ μm (mean ± S.D.) in the subcellular exposure, whereas those in the whole cell and for no exposure were $0.296 \pm 2.11$ μm and $0.630 \pm 1.69$ μm respectively. The minus value means the shift of the granule distribution towards the high glucose side.

## Discussion

The microfluidic device is driven by a single pump. This design allows the simple operation for cell trapping and robust subcellular delivery in comparison with a device driven by multiple pumps[13].
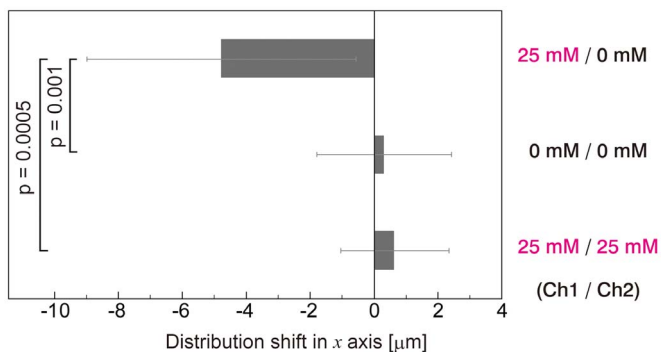


**Figure 5 | Shift of the spatial distribution, $X_{cell}'$, 4 h after subcellular glucose exposure.** The initial value is set to zero. The minus value indicates that the distribution shifts toward the high glucose side. Mean values ± standard deviation (S.D.). N = 12.

Although the trapped cells feel the pressure $P_{cell}$, it is still smaller than that in a typical patch clamp experiment (about 100 Pa[14]) and much smaller than the value when a cell raptures or passes through a micro-orifice (about 1000 Pa[14]). This estimation suggests that the pressure is small enough to keep the cells in their intact conditions. This is also supported by the fact that the trapped cells were alive and proliferated. The results of the delivery of the fluorescent solution (Fig. 2f) indicate that a trapped cell spreads at the orifice, covering or narrowing the gap between the cell and the wall of the orifice. This allowed us to keep a distinct difference in the chemical concentration between Ch1 and Ch2. The device developed here allows us to obtain the data of 1 or 2 cells per single experiment. Although the present device is not intended for the high-throughput analysis, it has a potential to increase the efficiency by arraying a large number of orifices in single chip and by integrating with a wide-field observation system, which will lead to a detailed analysis of single cells.

A pancreatic β-cell responds to a glucose solution whose concentration is higher than 5 mM. Glucose exposure induces the signal cascade to secrete insulin granules, involving the rise of the intracellular $[Ca^{2+}]$[15]. In living islets, it is thought that a β-cell is exposed to glucose nonuniformly and is stimulated partially at its surface. As far as we investigated the literatures, there is no report on the response of single pancreatic β-cells to subcellular stimulation. The time course of the subcellular stimulation (20 mM) in Fig. 3b shows an intracellular $[Ca^{2+}]$ rise similar to a typical response in a conventional bulk experiment where the cells are stimulated at their whole surface facing the aqueous solution[16]. This fact indicates that a cell in the microfluidic device keeps the function of the response to glucose stimulation; moreover, a β-cell can respond even though the glucose exposure area is very limited. The area of the cell surface where 20 mM glucose solution was delivered was estimated to be $104 \pm 54$ μm$^2$ (mean ± S.D.). This was about 11% of the total cell surface.

The results of the response of insulin granules (Fig. 5) show that only the subcellular glucose exposure biases the intracellular insulin granules, indicating that the phenomenon is caused by the nonuniform glucose environment, not by a physical effect. Further investigation will be required for elucidating the dynamics of the granules during the subcellular exposure and for clarifying the mechanism. A report suggested that LKB1 induces the formation of a β-cell polarity[20], although the mechanism and the other factors remain unknown. The glucose-induced bias found here will provide a new insight into the formation and the maintenance of the cell polarity in a living islet.

A β cell stores insulin granules in it at low glucose situation. Immediately after exposure to high glucose, the cell secretes them, thus the amount of intracellular insulin decreases. On the other hand, the production of insulin is up-regulated by glucose several hours after stimulation[21]. The amounts of insulin in our experiments were not altered substantially after 4 h exposure. The result suggests that the increase of the insulin production compensates the decrease of insulin induced by the secretion. To see more details about this and the dynamics of the insulin granules requires the increase of the time frame. We obtained only 2 time frames which is 0 h and 4 h. This is because the operations for the cell observation could disturb the flow pattern in the device and damage the cells by the pressure fluctuation at the orifices and by the excitation light. To minimize these impacts, we selected the limited time points in this paper. The integration of the subcellular exposure setup and the live-cell imaging system will allow the faster time frame, leading to the further understanding of the dynamics.

From the viewpoint of the technical aspects, the techniques and the materials developed here will be applicable to many studies. The insulin-GFP expressing cell line (MIN6m9-C4) will be a powerful tool for studies on the dynamics of insulin granules[22]. Regarding the microfluidic device, it readily produces a heterogeneous chemical environment and keeps it while delivering chemicals to a limited area of a single cell. Adapting the device to cell polarity studies will accelerates the *in vitro* understandings of how intracellular heterogeneities are induced by the chemical environment.

## Methods

**Microfluidic device.** The microfluidic device was fabricated using a soft lithography process[23] involving polydimethyl siloxane (PDMS). The details are shown in the Supplementary Data 1. First, a mold with a thickness of 20 μm, defining the height of the microchannels, was fabricated with SU-8 (MicroChem Corp.) on an Si substrate by standard UV lithography. Then, an acrylic polymer solution (Barrier Coat No.6, Shin-Etsu Chemical Co., Ltd.) was coated and dried there to form the meniscus bridges at the narrow gaps between the SU-8 structures as described in the literature[24]. The bridges have a circular shape in their cross sections, which were used as molds for forming circular micro-orifices. PDMS was poured onto the SU-8 mold and cured to transfer the structure. After being peeled off, the PDMS structure was treated with a corona discharge apparatus to be activated at the surface, bonded to a glass substrate (26 mm × 72 mm × 0.15 mm), and baked at 150°C for 2 h.

The device was bathed in phosphate-buffered saline (PBS) solution and put in a vacuum chamber, from which it was evacuated to remove the air bubbles in the channels. To improve the adhesion of the cells to the glass surface, we coated fibronectin molecules by washing with a solution of 4 μM fibronectin (Life Technologies Corp.) in PBS.

**Flow evaluation.** The flow in the device was evaluated with the finite element method (FEM) simulation. We used COMSOL Multiphysics ver.4.0 (COMSOL Inc.), adopting a 2D geometry model. The boundary conditions were set in accordance with the experimental situation, as follows. The two inlets have the same atmospheric pressure of a laminar flow influx. The velocity at the channel wall is zero. The outlet has a laminar flow outflux with a flow rate ranging from 0 to 5 μL/min. The mesh elements were triangular shape, whose details are as follows. Number of degrees of freedom, 2,668,927. Number of mesh elements, 582,232. Element area ratio, 1.48 × $10^{-9}$. We also simulated the situation when the trapped cells close all the orifices to estimate the pressure applied to them.

We visualized the actual flow pattern using fluorescent microparticles as tracers. Fluorescent polystyrene microparticles (Fluoresbrite YG Microspheres, Polysciences Inc.) of 1 μm in diameter were loaded into the two inlets. The flow was induced by the suction from the outlet at a flow rate of 2 μL/min by using a syringe pump (KD210, KD Scientific). The imaging system consisted of an inverted optical microscope (IX-71, Olympus Corp.) equipped with a Nipkow disk confocal laser scanner (CSU-X1, Yokogawa Electric Corp.), a solid-state 488-nm laser (Sapphire 488-75, Coherent Inc.), and an Electron-Multiplying charge-coupled device (CCD) camera (ImagEM C9100-13, Hamamatsu Photonics K.K.). The focus was adjusted in such a way to fit the observation plane to the center of the orifice. The images were processed with the ImageJ software to visualize the traces of the fluorescent particles and compare them to the streamlines predicted with the simulation.

We also verified the stability of the subcellular chemical delivery. After trapping and incubating mouse pancreatic β-cells (MIN6m9[25]) for 8 h at 37°C in a 5% $CO_2$ incubator, the device was placed on the microscope stage. Then, we applied a fluorescent solution consisting of 2 μM calcein-AM red orange (ex. 577 nm/em. 590 nm, Life Technologies Corp.)/PBS in Ch1 and suctioned it at the flow rate of 2 μL/min. We monitored the fluorescent intensity continuously in Ch1 and Ch2 around the

orifice for 4 h with the same observation setup as that used in the experiment for the visualization of fluorescent particles.

**Insulin-GFP–expressing cell line.** The vector provided from the Nagamatsu's group was transfected by lipofection into MIN6m9 cells. The construction of the vector was detailed in the literature[17]. We isolated six clones (C1–C6) expressing insulin-GFP molecules using the limiting dilution-culture method with the selection using neomycin. One clone (MIN6m9-C4) was selected among them, showing a bright insulin-GFP image and keeping the secretion function in response to glucose stimulation (details are given in the Supplementary Data 1). The cells were maintained in Dulbecco's modified Eagle's medium (DMEM, Gibco) containing 10% fetal bovine serum (FBS, Gibco) in a 5% $CO_2$ incubator at 37°C. Prior to the experiments in the device, the cells were cultured to 80% confluency in a culture dish and rinsed with PBS. Then, the cells were suspended by trypsin treatment (2.5% trypsin and 1 mM EDTA for 3 min in a 5% $CO_2$ incubator at 37°C). The suspended cells were aspirated and then centrifuged. The solution was replaced with fresh DMEM. Finally, the cell suspension ($1 \times 10^6$ cell/mL) was loaded into the microfluidic device.

**Imaging of the $[Ca^{2+}]$ response.** MIN6m9 cells were trapped and cultured in the microdevice. After the cells spread at the orifices, DMEM solution was replaced with a solution containing $[Ca^{2+}]$ fluorescent indicator, 2 μM Fluo-8 (ex. 490 nm/em. 512 nm, ABD Bioquest, Inc.)/glucose-free and calcium-free HEPES-added Krebs-Ringer bicarbonate buffer (HKRB) solution, and the mixture was incubated for 30 min in a 5% $CO_2$ incubator at 37°C for fluorescence staining. Then, it was rinsed with a fresh glucose-free HKRB solution. The device was placed on the stage of the inverted optical microscope and the syringe pump was connected to the outlet. The device was incubated in a transparent plate heater and a flexible sheet heater wound on an objective lens (ONICS, Tokai-hit Corp). The temperature of the solution was maintained at 36.0°C ± 1.0°C by monitoring it with a thermocouple microprobe (IT-23, AD Instruments Pty Ltd.). After a 20 mM glucose/HKRB solution was dispensed to a reservoir connected to Ch1, we immediately started the pump at the flow rate of 2 μL/min. The fluorescence of a trapped cell was observed through a 60× objective lens (UPLFLN, Olympus Corp.) for 30 min with the imaging system described in the flow evaluation section. After the imaging of the cell response was finished, we loaded a 2 μM calcein-AM red orange/PBS solution into Ch1 to identify which cell was stimulated and to check the leakage (Ch2 to Ch1) and the backflow (Ch1 to Ch2) of the solution through the orifice. We processed the images with the ImageJ software to plot the time course of the fluorescent intensity.

**Imaging of insulin granules.** The insulin-GFP expressing cells (MIN6m9-C4) established here were trapped in the microdevice in the same manner as for the $[Ca^{2+}]$ observation. After that, the solution in the channels was replaced with a glucose-free HKRB solution and incubated for 30 min in a 5% $CO_2$ incubator at 37°C. A glucose-free DMEM solution was applied to the two reservoirs to replace the solution in the device. Prior to the subcellular delivery, the cells were observed using the confocal imaging system described above. We used a 100×, 1.40 numerical aperture objective lens (UPLSAPO, Olympus Corp.) driven by a piezo-actuated z-scanner (P-720, PI GmbH & Co.) to capture the 3D stack image of insulin granules in a single cell, with the z spacing equal to 0.5 μm. The outlet was connected to the syringe pump and placed in a 5% $CO_2$ incubator at 37°C. After loading 25 mM glucose DMEM solution into the reservoir connected to Ch1, we immediately started the pump at the flow rate of 2 μL/min and stimulated the cells partially for 4 h. Then, the device was taken out from the incubator and placed on the microscope stage, where the insulin granules were observed again. We also performed the assays as control experiments by applying the same solution in both Ch1 and Ch2 (i.e., whole cell delivery). Although the diffusion of glucose in Ch2 for reaching a trapped cell requires about 300 s, it is much smaller than the glucose delivery time (4 h). Thus, we disregarded the effect. After the observation was finished, we applied calcein-AM red orange into Ch1 to identify the delivered cells and to check the flow.

The intracellular responses of the single cells were estimated from the change of the spatial distribution of insulin granules. We processed the 3D stack images of the insulin-GFP granules captured before and after the subcellular delivery. The images of the 3D stack were projected to a single 2D x-y image for the visualization of the x and y positions of all the granules existing in the single cell. The spatial distributions, $X'_{granule}$, were evaluated as described in the Results section. We subtracted the values of the initial state from those of 4 h delivery to obtain the shifts. Student's t-test assuming the unequal variances was used to evaluate the differences between the samples of the subcellular stimulation and the whole cell stimulation and between the subcellular stimulation and the no stimulation.

1. Goehring, N. W. & Grill, S. W. Cell polarity: Mechanochemical patterning. *Trends Cell. Biol.* **23**, 72–80 (2013).
2. Martin, K. C. & Ephrussi, A. mRNA localization: Gene expression in the spatial dimension. *Cell* **136**, 719–730 (2009).
3. Drubin, D. G. & Nelson, W. J. Origins of cell polarity. *Cell* **84**, 335–344 (1996).
4. Takayama, S. *et al.* Laminar flows - Subcellular positioning of small molecules. *Nature* **411**, 1016–1016 (2001).
5. Kuczenski, B., Ruder, W. C., Messner, W. C. & LeDuc, P. R. Probing cellular dynamics with a chemical signal generator. *Plos One* **4**, e4847 (2009).

6. Sawano, A., Takayama, S., Matsuda, M. & Miyawaki, A. Lateral propagation of EGF signaling after local stimulation is dependent on receptor density. *Dev. Cell* **3**, 245–257 (2002).

7. Juncker, D., Schmid, H. & Delamarche, E. Multipurpose microfluidic probe. *Nat. Mater.* **4**, 622–628 (2005).

8. Routenberg, D. A. & Reed, M. A. Microfluidic probe: a new tool for integrating microfluidic environments and electronic wafer-probing. *Lab on a Chip* **10**, 123–127 (2009).

9. Piper, J. D. *et al.* Characterization and application of controllable local chemical changes produced by reagent delivery from a nanopipette. *J. Am. Chem. Soc.* **130**, 10386–10393 (2008).

10. Tavana, H. *et al.* Nanolitre liquid patterning in aqueous environments for spatially defined reagent delivery to mammalian cells. *Nat. Mater.* **8**, 736–741 (2009).

11. Bonner-Weir, S. *Molecular and Cellular Biology of Diabetes Mellitus* Draznin, B. (ed) 1–11 (A.R. Liss, New York, 1989).

12. Bonner-Weir, S. Morphological evidence for pancreatic polarity of beta-cell within islets of Langerhans. *Diabetes* **37**, 616–621 (1988).

13. Terao, K. *et al.* Localized substance delivery to single cell and 4D imaging of its uptake using a flow channel with a lateral aperture. *Microfluid. Nanofluid.* **12**, 423–429 (2012).

14. Hamill, O. P. & McBride, D. W. Induced membrane hypo/hyper-mechanosensitivity: A limitation of patch-clamp recording. *Annu. Rev. Physiol.* **59**, 621–631 (1997).

15. MacDonald, P. E., Joseph, J. W. & Rorsman, P. Glucose-sensing mechanisms in pancreatic beta-cells. *Philos. Trans. R Soc. Lond. B Biol. Sci.* **360**, 2211–2225 (2005).

16. Yamada, K. *et al.* Measurement of glucose uptake and intracellular calcium concentration in single, living pancreatic beta-cells. *J. Biol. Chem.* **275**, 22278–22283 (2000).

17. Ohara-Imaizumi, M. *et al.* TIRF imaging of docking and fusion of single insulin granule motion in primary rat pancreatic beta-cells: different behavior of granule motion between normal and Goto-Kakizaki diabetic rat beta-cells. *Biochem. J.* **381**, 13–18 (2004).

18. Ohara-Imaizumi, M. *et al.* Imaging analysis reveals mechanistic differences between first- and second-phase insulin exocytosis. *J. Cell Biol.* **177**, 695–705 (2007).

19. Konstantinova, I. *et al.* EphA-ephrin-A-mediated beta cell communication regulates insulin secretion from pancreatic islets. *Cell* **129**, 359–370 (2007).

20. Granot, Z. *et al.* LKB1 regulates pancreatic beta cell size, polarity, and function. *Cell Metabolism* **10**, 296–308 (2009).

21. Vaulont, S., Vasseur-Cognet, M. & Kahn, A. Glucose regulation of gene transcription. *J. Biol. Chem.* **275**, 31555–31558 (2000).

22. Rorsman, P. & Renstrom, E. Insulin granule dynamics in pancreatic beta cells. *Diabetologia* **46**, 1029–1045 (2003).

23. Sia, S. K. & Whitesides, G. M. Microfluidic devices fabricated in poly(dimethylsiloxane) for biological studies. *Electrophoresis* **24**, 3563–3576 (2003).

24. Gel, M. *et al.* Microorifice-based high-yield cell fusion on microfluidic chip: Electrofusion of selected pairs and fusant viability. *IEEE Trans. NanoBiosci.* **8**, 300–305 (2009).

25. Minami, K. *et al.* Insulin secretion and differential gene expression in glucose-responsive and -unresponsive MIN6 sublines. *Am. J. Physiol. Endocrinol. Metab.* **279**, E773–E781 (2000).

## Acknowledgments

## Author contributions

K.T. together with T.O., M.W. and H.K. designed the study. K.T. together with M.G. and T.S. developed the device. T.T. and S.N. established the insulin-GFP expressing cell lines and K.T. characterized them by TIRF microscopy. A.O. and A.F. performed cell culture in the device. K.T. and A.F. performed the imaging of the cell response. K.T. analyzed the data and composed the manuscript.

## Additional information